Extended wave-packet model to calculate energy-loss moments of protons in matter

C. D. Archubi[*]

Consejo Nacional de Investigaciones Científicas y Técnicas – Universidad de Buenos Aires,
Instituto de Astronomía y Física del Espacio, Pabellón IAFE, 1428 Buenos Aires, Argentina
and Universidad de Buenos Aires, Facultad de Ciencias Exactas y Naturales, Departamento de Física,
Ciudad Universitaria, 1428 Buenos Aires, Argentina

N. R. Arista[†]

Centro Atómico Bariloche and Instituto Balseiro and Comisión Nacional de Energía Atómica, 8400 S. C. de Bariloche, Argentina

In this work we introduce modifications to the wave-packet method proposed by Kaneko to calculate the energy-loss moments of a projectile traversing a target which is represented in terms of Gaussian functions for the momentum distributions of electrons in the atomic shells. These modifications are introduced using the Levine and Louie technique to take into account the energy gaps corresponding to the different atomic levels of the target. We use the extended wave-packet model to evaluate the stopping power, the energy straggling, the inverse mean free path, and the ionization cross sections for protons in several targets, obtaining good agreements for all these quantities on an extensive energy range that covers low-, intermediate-, and high-energy regions. The extended wave-packet model proposed here provides a method to calculate in a very straightforward way all the significant terms of the inelastic interaction of light ions with any element of the periodic table.

I. INTRODUCTION

The physics of the interaction of ions with matter is a subject of great scientific interest, with large impact on basic and applied research, being also the basis of numerous applications, such as ion-beam analysis, particle-induced x-ray emission, ion implantation, space physics, radiation effects, medical physics, and many others. Recent surveys in the field show a great level of activity and provide a large amount of information [1–3]. The list of scientific works in the field is large; relevant information, including earlier work and recent advances, can be found in Refs. [4–14]. Extended compilations of experimental data are also available [15,16]. From the theoretical side, influential works in this area were done by Bethe [17], Fermi [18], Lindhard [19], Ritchie [20], and others. In particular, theoretical approaches have been developed to describe the characteristic values of the interaction processes, including calculations of the mean energy loss, or stopping power, energy straggling, inelastic mean free paths, and ionization cross sections [8,9]. Among the earlier models [17–20], the interesting advantage of the Lindhard dielectric formulation [19] is that it yields a full description of the velocity dependence, going from low to high speeds (in the nonrelativistic range) and describing the stopping power maximum. However, it has two basic limitations: (i) it considers a free-electron gas (Sommerfeld model), which in principle restricts the applicability to conduction electrons in ideal metals, and (ii) it is a linear model, so it does not take into account nonlinear effects that are particularly important at low energies [21–24].

In the 1990s, Kaneko presented a new theoretical approach to calculate the stopping power of bound electrons [25–27], whose internal system was described in momentum space as a dense interacting electron gas with a Gaussian occupation probability. This new approach proposed an alternative type of random-phase-approximation (RPA) dielectric function and was given the name of *wave-packet model* (WPM). It has some of the general properties of Lindhard's model (LM) but extends its domain of application to different target systems. The WPM provides a significant advantage in terms of analyticity and can be applied in principle to all atomic shells and elements of the periodic table. Both the LM and WPM were designed following the quantum (RPA) dielectric function approach (and so both are of perturbative nature) and bear similarities in terms of analytical properties, the main difference being that while Lindhard's model applies to a degenerate free-electron gas, described in terms of plane waves, the WPM considers Gaussian distributions of electron speeds. Thus, the Lindhard model applies most naturally to conduction electrons in metals whereas Kaneko's model provides a better approach to atomic-shell electrons.

One of the restrictions of both LM and WPM is the absence of energy gaps or binding effects, so that electrons can be excited as free particles and may be detached from the condensed state without spending the minimum energy corresponding to the band gaps in semiconductors or insulators (in the LM) or the ionization energy in atomic shells (in the WPM). In particular, in the WPM case to be considered here, the velocity distributions are appropriate to describe atomic shells but the electrons are in other aspects considered as free particles, and may be easily removed without the restrictions of ionization thresholds. A consequence of this is that at low energies the stopping power of each atomic shell shows a linear velocity behavior down to very low velocities.

[*]archubi@iafe.uba.ar
[†]arista@cab.cnea.ar

From a different line of research, Levine and Louie (LL) [28] proposed a general method to introduce the effects of energy gaps within the context of the quantum dielectric function formalism. This approach has the great advantage of maintaining all the pertinent sum rules that characterize the quantum dielectric response formalism. In a recent set of papers [29,30] we used a combination of the Lindhard and LL models to study the band-gap effects in the excitation of valence electrons in semiconductors and insulators and extended the comparisons to the cases of protons, electrons, and positrons. This combination of LM and LL models provides a convenient way to describe and compare these various projectile-target combinations with a unified approach [30,31].

These previous developments serve as a motivation for the present study. The central idea of this work is to make use of the analytical properties and wide possibilities of Kaneko's wave-packet model, with the important amendment of considering the binding energies of atomic shells, which is done using the Levine-Louie method. The result of this is the extended wave-packet model (EWPM), an approach that allows one to calculate the characteristic values of inelastic processes (stopping power, energy straggling, inverse mean free paths, and ionization cross sections) in a very general and straightforward way.

The present work is organized as follows: In Sec. II we describe the dielectric approach used in this study. In Sec. III we extend this approach considering the binding energies of atomic shells. In Sec. IV we present the expressions for the various energy-loss moments and the emission cross section. In Sec. V we show the results of the calculations of the energy-loss moments and the ionization cross section for protons comparing the EWPM results with the experiments and with those results obtained using the WPM. The conclusions are summarized in Sec. VI.

II. KANEKO'S WAVE-PACKET MODEL

The main assumption of this model is the consideration of Gaussian distributions for the electron velocities of a given atomic shell, i.e., $f(v) \approx e^{-v^2/\overline{v}^2}$, where $\overline{v}$ is a characteristic speed of the considered shell. The dielectric function for this system is described in terms of a characteristic wave vector $\overline{q}$, which is related to $\overline{v}$ by $\hbar\overline{q} = m_e\overline{v}$. The value of $\overline{q}$ is determined by the relation $\overline{q} = q_1 N^{1/3}$, where N is the number of electrons in the shell and q_1 is a shell parameter whose value is determined from Hartree-Fock calculations of electron velocity distributions using the results of previous authors [32,33].

A. Dielectric function

By assuming Gaussian distributions of electron speeds, the wave-packet model yields closed analytical expressions for the real and imaginary parts of the dielectric function $\epsilon(k,\omega) = \epsilon_1(k,\omega) + i\epsilon_2(k,\omega)$, where k and ω are the wave-vector and frequency variables. The results for ϵ_1 and ϵ_2 may be cast in a convenient way in terms of the dimensionless variables $u = \omega/k\overline{v}$ and $z = k/2\overline{q}$ (which are analogous to Lindhard's

u,z variables) as follows [25]:

$$\epsilon_1(u,z) = 1 + \gamma\frac{\chi^2}{z^2}\frac{1}{8z}[F(u+z) - F(u-z)], \quad (1)$$

$$\epsilon_2(u,z) = \gamma\frac{\chi^2}{z^2}\frac{\pi}{8z}[e^{-(u-z)^2} - e^{-(u+z)^2}], \quad (2)$$

where the parameter $\chi^2 = e^2/\pi\hbar\overline{v}$.

The function $F(x)$ is defined by

$$F(x) = \sqrt{\pi}K(x) = \sqrt{\pi}\int_0^\infty \sin(tx)e^{-t^2/4}dt. \quad (3)$$

An alternative expression for $K(x)$ (more useful for numerical calculations) is

$$K(x) = \frac{\varphi(\sqrt{2}x)}{x}, \quad (4)$$

where

$$\varphi(x) = x\int_0^x e^{(t^2-x^2)/2}dt. \quad (5)$$

Finally, we have introduced a parameter γ in Eqs. (1) and (2) which was not present in the original Kaneko model (so $\gamma = 1$ in that case). The use of this parameter is explained later on.

III. EXTENDED WAVE-PACKET MODEL

We introduce now the effect of energy binding in the wave-packet formulation using the method proposed by Levine and Louie [28]. The LL method consists in performing a shift in the frequency variable by the replacement $\omega \rightarrow \sqrt{\omega^2 - \omega_0^2}$, where $\omega_0 = I_s/\hbar$ and I_s is an energy gap, which in the present case is the binding energy of a given atomic shell.

Specifically, the new dielectric function $\widetilde{\epsilon}$ becomes, for $\omega > \omega_0$,

$$\widetilde{\epsilon}_1(k,\omega) = \epsilon_1\big(k,\sqrt{\omega^2 - \omega_0^2}\big), \quad (6)$$

$$\widetilde{\epsilon}_2(k,\omega) = \epsilon_2\big(k,\sqrt{\omega^2 - \omega_0^2}\big), \quad (7)$$

whereas for $\omega < \omega_0$, $\widetilde{\epsilon}_2(k,\omega) = 0$, while $\widetilde{\epsilon}_1(k,\omega)$ is obtained from $\widetilde{\epsilon}_2(k,\omega)$ using the Kramers-Kronig relations. In this way, the LL method opens a gap in the map of excitations such that inelastic processes occur only for frequencies $\omega > \omega_0$. For this reason, all the quantities calculated here will be obtained from integrals in the domain $\omega > \omega_0$, where the values of $\widetilde{\epsilon}_1$ and $\widetilde{\epsilon}_2$ can be expressed analytically in terms of Eqs. (1)–(7). We refer to this approach as the extended wave-packet model.

A. Sum rules

As is well known, the dielectric function for a free-electron gas (FEG) satisfies the sum rules

$$\int_0^\infty \epsilon_2(k,\omega)\omega \, d\omega = \frac{\pi}{2}\omega_p^2 \quad (8)$$

and

$$\int_0^\infty \mathcal{F}_{\mathrm{EL}}(k,\omega)\omega \, d\omega = \frac{\pi}{2}\omega_p^2, \quad (9)$$

where ω_p is the plasma frequency of the electron gas, and $\mathcal{F}_{\mathrm{EL}}(k,\omega)$ denotes the energy-loss function defined by $\mathcal{F}_{\mathrm{EL}}(k,\omega) = \epsilon_2(k,\omega)/|\epsilon(k,\omega)|^2$.

In the present case, using the expressions for $\widetilde{\epsilon}_1$ and $\widetilde{\epsilon}_2$ given before and performing the frequency integrals we obtain

$$\int_0^\infty \widetilde{\epsilon}_2(k,\omega)\omega\,d\omega = \frac{\pi^{3/2}}{2}\gamma\,\chi^2(\overline{qv})^2, \tag{10}$$

and the same value is obtained for the corresponding energy-loss function.

Therefore we define an equivalent plasma frequency by

$$\overline{\omega}_p^2 = \pi^{1/2}\gamma\,\chi^2(\overline{qv})^2 \tag{11}$$

(in atomic units this relation is simply given by $\overline{\omega}_p^2 = \gamma\overline{q}^3/\sqrt{\pi}$).

It should be noted, however, that this frequency is different for each atomic shell. As in the case of the free-electron gas, the value of the sum rules is the same and is independent of the value of k, and this remarkable property is satisfied both by the original wave-packet model as by the extended one. This is one of the significant properties of these models.

IV. INTEGRALS FOR THE ENERGY-LOSS MOMENTS

We are here interested in calculating the main moments of the energy-loss distribution, which are given by the integrals (with $n = 0,1,2,...$)

$$Q_n = \frac{2}{\pi}\left(\frac{Ze}{v}\right)^2\hbar^{n-1}\int_0^\infty \frac{dk}{k}\int_0^{kv}\omega^n\,\mathrm{Im}\left[\frac{-1}{\widetilde{\epsilon}(k,\omega)}\right]d\omega, \tag{12}$$

where Ze and v are the charge and velocity of the incident particle. The units of Q_n are *(energy)^n/length*.

This expression of Q_n yields the values of the inverse inelastic mean free path, stopping power, and straggling, when $n = 0,1$, and 2, namely,

(i) inverse inelastic mean free path (IMFP): $1/\lambda_i = Q_0$,
(ii) stopping power: $S = |\langle dE/dx\rangle| = Q_1$,
(iii) energy straggling: $\Omega^2 = \langle\delta E^2\rangle/dx = Q_2$.

Another quantity of interest is the ionization cross section, which is directly related to the inelastic mean free path λ_i by

$$\sigma_i = \frac{1}{n_a\lambda_i}, \tag{13}$$

where n_a is the atomic density.

Using the reduced variables $u = \omega/k\overline{v}$ and $z = k/2\overline{q}$, the Q_n integral becomes

$$Q_n = \frac{2}{\pi}\left(\frac{Ze}{v}\right)^2\hbar^{n-1}(2\overline{qv})^{n+1}\int_0^\infty z^n\,dz$$

$$\times \int_0^{v/\overline{v}}\mathrm{Im}\left[\frac{-1}{\widetilde{\epsilon}(u.z)}\right]u^n\,du. \tag{14}$$

Several examples of calculations for specific cases are considered in the next section.

V. CALCULATIONS

A. Stopping power

Since the previous calculations with the wave-packet model were concentrated in the stopping power, which is the most studied energy-loss parameter, both experimentally and theoretically, we start the analysis by considering this quantity.

Figure 1 shows the separated contributions to the stopping cross section for the case of protons traversing an Al target. To represent the conduction band we calculated the stopping cross section for a free-electron gas characterized by a Wigner-Seitz radius $r_s = 2.07$ using both the Lindhard model and the nonlinear transport cross-section model [24]. These calculations for a free-electron gas include the contribution of collective excitations (plasmons), either as a separate mechanism or by a self-consistent approach. The results for the conduction band, which correspond to the dominant contribution at low velocities, show that nonlinear effects become non-negligible and must be taken into account. In order to permit the visualization of the inner-shell contributions in this figure, the results for the conduction (free-electron) band have been divided by 3. When calculating the inner-shell contribution with both models, WPM and EWPM, we have analyzed the possible contribution of resonant collective excitations of bound electrons, but we found it negligible (this has also been noted earlier by Kaneko [26]).

The pair of curves for the $1s$, $2s$, and $2p$ shells in Fig. 1 shows the results of the two versions of the wave-packet model using the Gaussian parameters q_1 tabulated by Kaneko [27], which were obtained from Hartree-Fock calculations of momentum distributions for each shell [32]. The only difference between the WPM and EWPM results stems from the consideration of the binding energies I_s of each shell in the latter case. The figure clearly shows that the effect of introducing a binding energy is a reduction of the
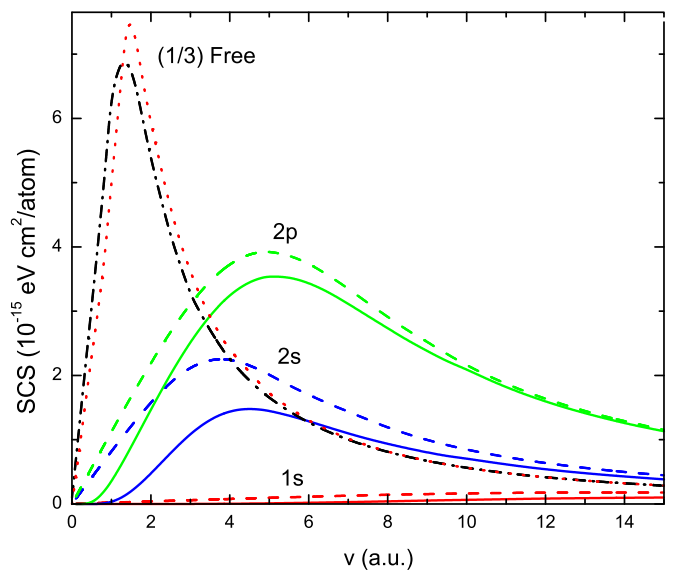
FIG. 1. Separated contributions to the stopping cross section for protons in an Al target as a function of the projectile velocity. Dashed lines: WPM. Full lines: EWPM. Dotted line: Lindhard's free-electron gas. Dashed-dotted line: nonlinear results for the free-electron gas.
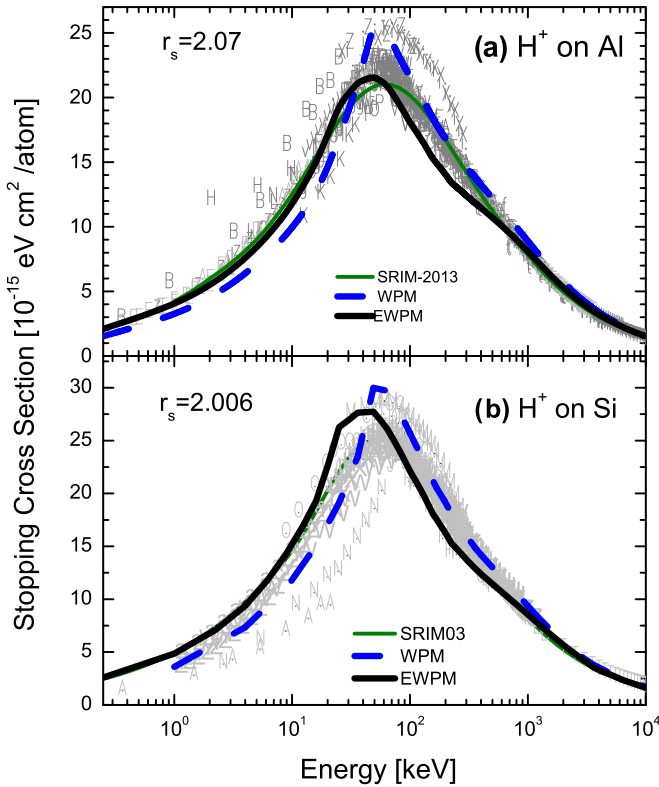
FIG. 2. Stopping cross section for protons as a function of the projectile energy: (a) Al target and (b) Si target. Thick dashed lines: WPM. Thick full lines: EWPM. Symbols: Experimental data extracted from [16].

FIG. 3. Stopping cross section for protons as a function of the projectile energy in transition metals: (a) Ag target and (b) Au target. Dashed-dotted line in panel (b): theoretical calculations by Montanari *et al.* [35]. Thick dashed lines: WPM. Thick full lines: EWPM. Symbols: Experimental data extracted from [16].

contributions of all the inner shells. This is understandable because to transfer energy to bound electrons, the projectile must overcome the corresponding energy thresholds.

To illustrate these results in a more realistic way, we include in Figs. 2 and 3 a set of calculations and comparisons with experimental results for several representative cases of particular interest. In Fig. 2 we show the total stopping cross section calculated with the WPM and EWPM for two light targets: (a) Al and (b) Si. The experimental results together with the semiempirical SRIM curves shown in this figure have been extracted from Paul's data tabulations [16]. In both cases, the results obtained with the EWPM produces a small improvement in the shape of the curves, although we notice a depletion in the values just over maximum in the case of Al (related to a threshold effect in the ionization of the $2s$ and $2p$ shells) and a shift in the position of the maximum for Si. These differences may indicate some misadjustments in the velocity distributions of the outer shells with respect to the tabulated HF values for free atoms. A variation of those parameters may improve the quality of this comparison, but we leave this question open to separate investigation. In the EWPM calculations we used the nonlinear results for the conduction band, which improves the agreement at low energies.

In Fig. 3 we analyze the interesting case of transition metals for two characteristic heavier atoms: (a) Ag and (b) Au. We include here two EWPM calculations (EWPM-1 and EWPM-2 curves): the first one is the result obtained with this model using the q_1 according to the Hartree-Fock values as indicated

before [27,32]. As it may be observed for both elements, the WPM and EWPM-1 results do not agree well with the experiments, showing a similar distortion in the shape of the stopping power curves. For this reason we endeavored to a more particular analysis. In the cases of Ag and Au, as well as other transition metals, there is an important contribution from d electrons. As is well known, these electrons have particular band-structure properties that cannot be represented by the standard Hartree-Fock (HF) description corresponding to free atoms [32,33]. In fact, in the solid-state phase these electrons are weakly bound, and the corresponding density of states shows a rather broad distribution [34]. This produces some particular threshold effects in the low-energy stopping power, as previous studies revealed [36]. We think this is the reason why the contribution of the d electrons is not well described by the standard WPM or EWPM when the atomic HF parameters are used. Therefore, we considered a possible way to adapt the wave-packet model to the case of d electrons by a variation in the value of the Gaussian parameter q_1, used in the wave-packet formulation, to allow a wider velocity distribution than that predicted by the atomic HF calculations. However, when doing this modification it is important to assure that the value of the sum rules is not affected. This is the reason why we introduced the parameter γ in Eqs. (1) and (2), which permits us to tune the value of the equivalent plasma frequency and hence the value of the sum rule. Therefore, in the cases of Ag and Au we changed simultaneously the parameters q_1 and γ,

maintaining the value of the sum rules constant. The results of these calculations are the EWPM-2 curves shown in the figure. We found a fairly good agreement with the experiments using the following values: $q_1 = 0.53$, $\gamma = 2.69$, for the $4d$ electrons of Ag, and $q_1 = 0.5$, $\gamma = 2.993$, for the $5d$ electrons Au (whereas the HF values of q_1 for these cases are 0.737 and 0.7206, respectively). A binding energy of 4 eV was used in these cases, representing the properties of weakly bound states, in accord with the density of states of both metals [34]. The result of these calculations are shown in Fig. 3 by the curves denoted EWPM-2. These new calculations show a smoother behavior and a better agreement with the experimental results.

We conclude from this particular study that the d electrons play an important role in these cases, and the way in which they are represented can modify the shape of the stopping curve. In addition, we observe that the WPM and EWPM can still be adapted to account in an approximate way for these effects.

Finally, in Fig. 4 we show the behavior of both contributions for the cases of Au and Ag targets: FEG calculated with the nonlinear method and the atomic shells calculated with EWPM model. We have included the separate results for the dominant last shells. A comparison between Fig. 1 and Fig. 4 clearly shows that in these last cases the sum of the contributions of the atomic shells represents a greater percentage of the total
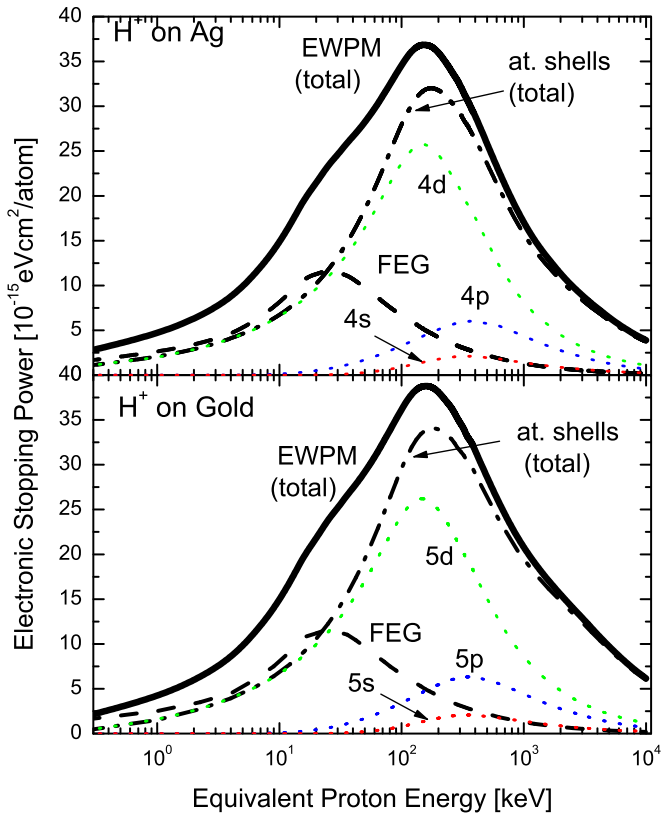
FIG. 4. Separated contributions to the stopping cross section for protons in Ag and Au targets as a function of the projectile velocity. Full line: EWPM-2 (total result). Dashed lines: nonlinear results for the free-electron gas. Dashed-dotted line: total contribution of the atomic shells calculated with EWPM-2. Dotted lines: separate contributions for the last atomic shells.
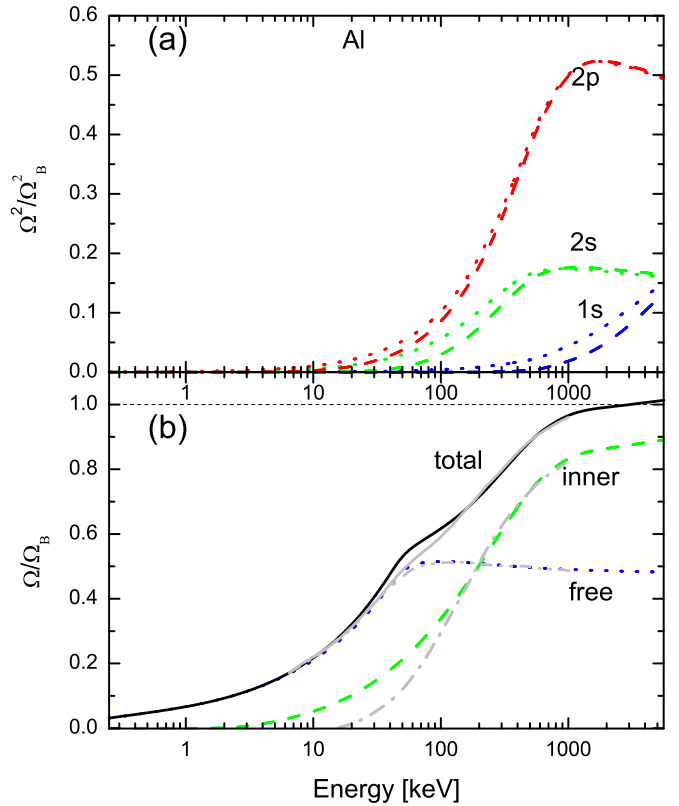
FIG. 5. Inner-shell and free-electron gas contributions to relative straggling for protons as a function of the projectile energy in Al. (a) Dotted lines: WPM; dashed lines: EWPM. (b) Contributions from inner shells and free electrons, and total energy straggling, obtained with the EWPM; the gray lines show the corresponding results of Arbó *et al.* [38] using the CDW-EIS approximation.

results than in the case of Al. Thus, the EWPM model becomes more important to determine an appropriate comparison with the experiments.

B. Straggling

We now turn to the analysis of the second moment of the energy-loss distribution, i.e., the energy straggling. In Fig. 5 we show the characteristics of the straggling contributions from the various shells of Al. We use as a reference the value of the Bohr straggling, Ω_B, which represents the well-known asymptotic value [37]. In part (a) of this figure we show the separate contributions of the $1s$, $2s$, and $2p$ shells, where in each case the pair of curves shows the values of the WPM and EWPM calculations. As in the case of the stopping power, we obtain a diminution in the values due to the effect of the energy binding for each shell. In Fig. 5(b) we show the sum of the inner-shell contributions [$\Omega_{\text{inner}} = (\Omega_{1s}^2 + \Omega_{2s}^2 + \Omega_{2p}^2)^{1/2}$], the contribution of the Al free electrons (Ω_{free}), and total straggling [$\Omega_{\text{total}} = (\Omega_{\text{inner}}^2 + \Omega_{\text{free}}^2)^{1/2}$]. The gray line in this figure shows a previous calculation of the straggling using the CDW-EIS approximation method [38]. We observe that, as for the stopping cross section, the dominant contribution for low energies is given by the free-electron gas, but inner-shell contributions to the straggling become dominant when the projectile energy increases, overcoming the thresholds
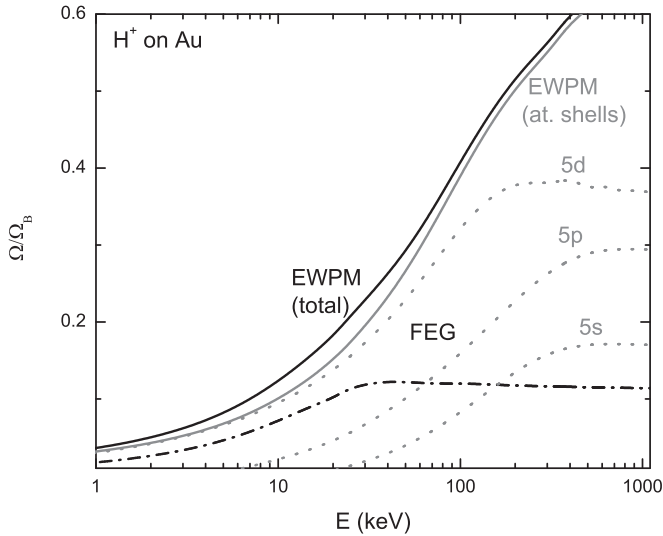
FIG. 6. Atomic-shell and free-electron gas contributions to relative straggling for protons as a function of the projectile energy in Au. Full line: EWPM-2 (total result). Dashed-dotted line: nonlinear result for the FEG. Gray full line: total atomic-shell contribution. Gray dotted lines: contributions from the last dominant atomic shells.

corresponding to each individual binding energy of the atomic shells. The excellent agreement with the much more sophisticated CDW-EIS calculations is remarkable.
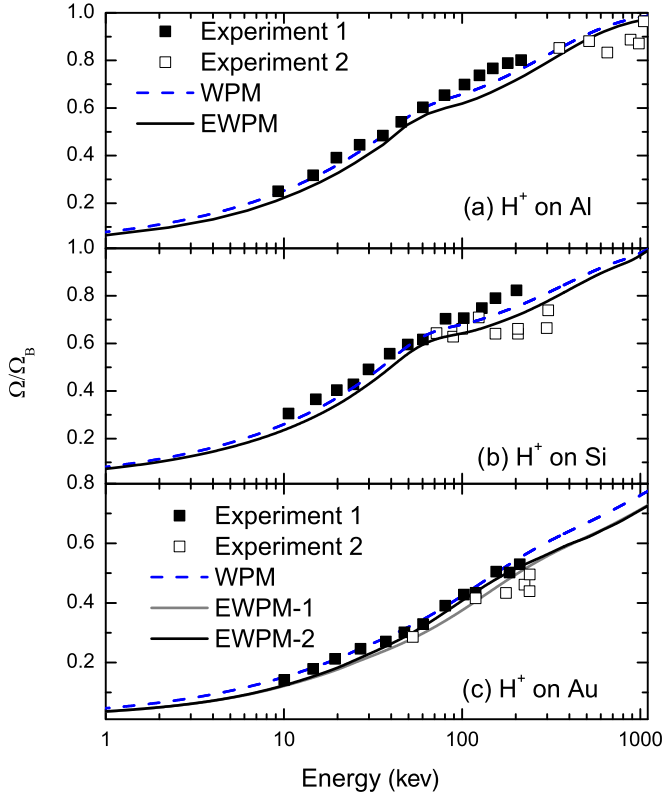
FIG. 7. Relative straggling for protons as a function of the projectile energy in different targets: (a) Al, (b) Si, and (c) Au. Full squares: Experimental data extracted from [38]. Open squares: Experimental data extracted from [39–41].
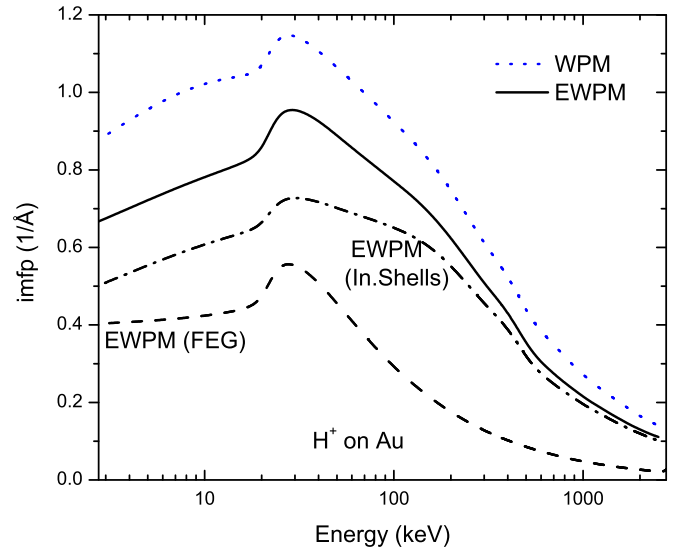
FIG. 8. Inverse mean free path for protons traversing an Au target as a function of the projectile energy. Total values according to the WPM and EWPM, and contributions from inner shells and free electrons using the EWPM.

Figure 6 shows the results for the case of Au. The contribution of the atomic shells to the total result is more important than for Al, as it was expected from the analysis of the same behavior for stopping. Moreover, Fig. 6 shows that this contribution to the straggling is dominant in all the range of energies.

In Fig. 7 we compare the results of the present EWPM calculations with the experimental values of Refs. [38,39,41], for Al, Si, and Au. In these cases, both the WPM and EWPM results are in good agreement with the experiments; this shows that the straggling is a less sensitive magnitude with respect to energy-binding effects.
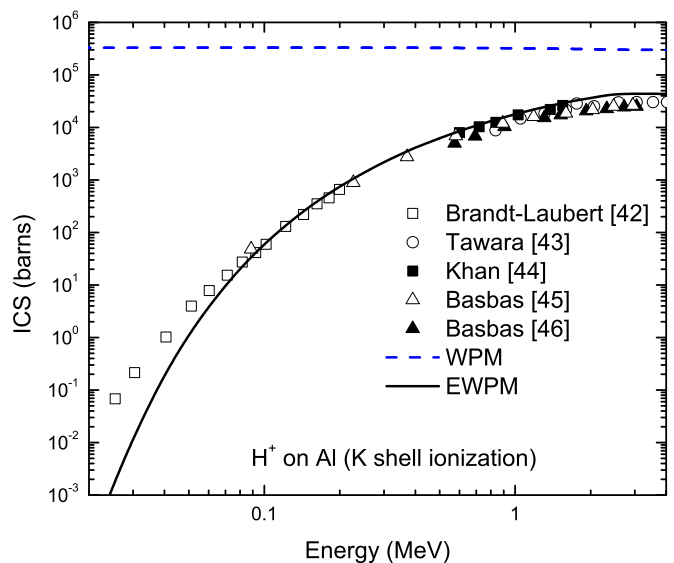
FIG. 9. K-shell ionization cross section for protons traversing an Al target as a function of the projectile energy. Squares, triangles, and circles: Experimental data.

C. Inverse mean free path and ionization cross sections

As a final test of the EWPM, we consider now the calculation of inelastic inverse mean free paths (IMFP) and inelastic cross sections (ICS). These quantities are highly sensitive to energy-binding effects; therefore, these calculations provide a very stringent numerical test to the present approach.

In Fig. 8 we show the results of IMFP calculations for H^+ on Au targets. We separate in this figure the contributions of the free-electron gas and of the inner shells. As it may be observed, the inner-shell contribution is dominant on the whole energy range. The solid line in this figure is the value of the total IMFP obtained with the EWPM, while the blue dotted line is the total IMFP calculated with the WPM. This shows that the binding effects produce a strong reduction of the IMFP values. As indicated by Eq. (13), the IMFP terms and the corresponding ICS's are directly related. But in the case of protons the experiments directly determine the values of the cross sections [42–49]. Therefore we concentrate here on ICS values for various inner shells and elements where experimental results are readily available. In Fig. 9 we show the calculations of the ionization cross section for the K shell

of Al and compare it with experimental values from different sources [42–46]. We find a very good agreement, except for the lower energy range where the theoretical EWPM curve drops too rapidly. The blue dotted line in this figure is the ICS value calculated with the original WPM, which does not consider energy-binding effects and shows too large and nearly constant values. We notice here that the binding effects amount to several orders of magnitude (from 1 to around 6 orders) on the whole energy range. A set of similar calculations is shown in Fig. 10, including the K and L shells of Si [43,47], the K shell of Cu [48], and the L and M shells of Au [49]. In all the cases (with the exception of the L shell of Si) the magnitude of the binding effects is also very large and in accord with the values of the binding energies for the inner shells. We may stress here that the theoretical values show good agreement with the experiments, reproducing the results over a range of ICS from 1 barn up to 10^7 barns. We also observe a systematic discrepancy for the L shell of Si, which may bear some relation with the previously noticed differences in the stopping power values in Fig. 2. This seems to confirm the previous consideration that a more extensive study of the HF parameters for the outer shells used in the wave-packet model could lead to further improvements in the final numerical tests.
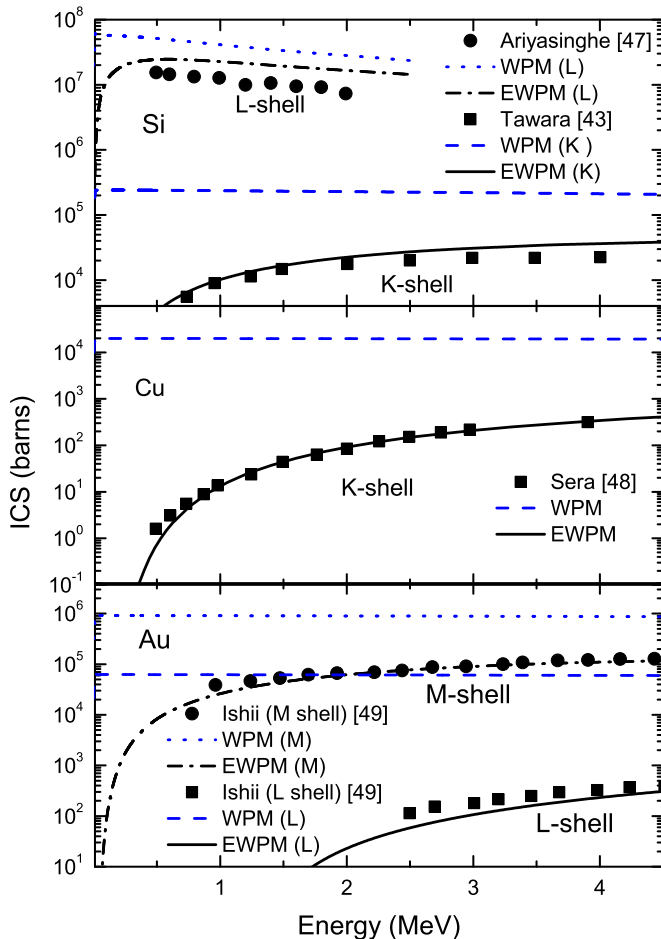
VI. CONCLUSIONS

The original wave-packet model proposed by Kaneko brings the possibility of representing the kinematic properties of inner shells in terms of Gaussian distributions of electron speeds. This provides a convenient framework to achieve a very general description of the energy loss of charged particles or related quantities. The original model accounts for the shell corrections to the stopping power but does not include the corresponding binding effects of the atomic shells. In this work we extended the wave-packet model by incorporating those binding effects through a very general formulation that conserves the exact sum rules, and it requires as the only additional ingredient the values of the binding energy for each shell. This yields a powerful method that can be used to calculate the main parameters characterizing the interaction of protons or other light ions with almost any atomic shell (without considering relativistic effects), and allows a straightforward application for all atoms in the periodic table. We have illustrated this approach by calculations of stopping powers, energy straggling, mean free paths, and ionization cross sections for various representative elements. A good general agreement with experiments was obtained, comparable with that obtained by calculations with more sophisticated methods. We find some irregularities in the stopping-power results for transition elements such as Ag and Au, which we consider related to the special band-structure properties of the d-electron bands of those elements. The results for the ionization cross sections show a good agreement, covering many orders of magnitude in the results for K, L, and M shells of typical elements. We think this method can be used with perhaps great advantages in many future developments, remaining open to the possibility of modifying our model to investigate significant areas of current interest, such as the stopping of protons in compounds, the stopping of helium projectiles, the study of phase effects, and the significance of

FIG. 10. Ionization cross sections for protons traversing different targets: (a) Si: K and L shells, (b) Cu: K shell, and (c) Au: L and M shells. Full squares and circles: Experimental data from different sources.

Bragg's rule. As far as we know, this is the only general method that provides immediate theoretical values for all the moments of the energy loss, or inelastic interaction terms, for any target element of the periodic table, without recourse to cumbersome computations. Further calculations and applications to other cases of interest will be considered elsewhere.

[1] *Ion Beam Analysis: Fundamentals and Applications*, edited by M. Nastasi, J. W. Mayer, and Y. Wang (CRC Press, Boca Raton, FL, 2014).

[2] *Handbook of Modern Ion Beam Materials Analysis*, 2nd ed., edited by Y. Wang and M. Nastasi (Cambridge University Press, Cambridge, UK, 2011), Vol. 1.

[3] *Ion Beams in Materials Processing and Analysis*, edited by B. Schmidt and K. Wetzig (Springer, New York, 2012).

[4] U. Fano, Penetration of protons, alpha particles, and mesons, Annu. Rev. Nucl. Sci. **13**, 1 (1963).

[5] F. Inokuti, Inelastic collisions of fast charged particles with atoms and molecules–The Bethe theory revisited, Rev. Mod. Phys. **43**, 297 (1971).

[6] S. P. Ahlen, Theoretical and experimental aspects of the energy loss of relativistic heavily ionizing particles, Rev. Mod. Phys. **52**, 121 (1980).

[7] *Energy Loss and Ion Ranges in Solids*, M. A. Kumakhov and F. F. Komarov (Gordon and Breach, New York, 1981).

[8] *Interaction of Charged Particles with Solids and Surfaces*, edited by A. Gras-Martí, H. M. Urbassek, N. R. Arista, and F. Flores (Plenum Press, New York, 1991).

[9] *Theory of the Interaction of Swift Ions with Matter*, edited by R. Cabrera-Trujillo and J. Sabin, Advances in Quantum Chemistry Vol. 45 (Elsevier, New York, 2004), Chap. 3.

[10] *Particle Penetration and Radiation Effects*, edited by P. Sigmund (Springer, New York, 2006).

[11] A. P. Horsfield, A. Lim, W. M. C. Foulkes, and A. A. Correa, Adiabatic perturbation theory of electronic stopping in insulators, Phys. Rev. B **93**, 245106 (2016).

[12] E. E. Quashie, B. C. Saha, and A. A. Correa, Electronic band structure effects in the stopping of protons in copper, Phys. Rev. B **94**, 155403 (2016).

[13] M. A. Zeb, J. Kohanoff, D. Sanchez-Portal, A. Arnau, J. I. Juaristi, and E. Artacho, Electronic Stopping Power in Gold: The Role of d Electrons and the H/He Anomaly, Phys. Rev. Lett. **108**, 225504 (2012).

[14] D. Roth, B. Bruckner, M. V. Moro, S. Gruber, D. Goebl, J. I. Juaristi, M. Alducin, R. Steinberger, J. Duchoslav, D. Primethzhofer, and P. Bauer, Electronic Stopping of Slow Protons in Transition and Rare Earth Metals: Breakdown of the Free Electron Gas Concept, Phys. Rev. Lett. **118**, 103401 (2017).

[15] *The Stopping and Range of Ions in Solids*, J. Ziegler, J. P. Biersack, and U. Littmark (Pergamon, New York, 1985); cf. also full tabulations at http://www.srim.org.

[16] Stopping Power of Matter for Ions, Graphs, Data, Comments and Programs, https://www-nds.iaea.org/stopping/.

[17] H. Bethe, Zur theorie des durchgangs schneller Korpuskularstrahlen durch materie, Ann. Phys. **397**, 325 (1930).

[18] E. Fermi, The ionization loss of energy in gases and in condensed materials, Phys. Rev. **57**, 485 (1940).

[19] J. Lindhard, On the properties of a gas of charged particles, Mat. Fys. Medd. Dan. Vid. Selsk **28**, 1-57 (1954).

[20] R. H. Ritchie, Interaction of charged particles with a degenerate Fermi-Dirac electron gas, Phys. Rev. **114**, 644 (1959).

[21] T. L. Ferrell and R. H. Ritchie, Energy losses by slow ions and atoms to electronic excitation in solids, Phys. Rev. B **16**, 115 (1977).

[22] A. Mann and W. Brandt, Material dependence of low-velocity stopping powers, Phys. Rev. B **24**, 4999 (1981).

[23] P. M. Echenique, R. M. Nieminen, and R. H. Ritchie, Density functional calculation of stopping power of an electron gas for slow ions, Solid State Commun. **37**, 779 (1981).

[24] N. R. Arista, Energy loss of ions in solids: Non-linear calculations for slow and swift ions, Nucl. Instrum. Methods Phys. Res., Sect. B **195**, 91 (2002).

[25] T. Kaneko, Wave packet theory of bond electrons, Phys. Rev. A **40**, 2188 (1989).

[26] T. Kaneko, Partial and total electronic stoppings of solids and atoms for energetic ions, Phys. Status Solidi B **156**, 49 (1989).

[27] T. Kaneko, Partial and electronic stopping cross sections of atoms and solids for protons, At. Data Nucl. Data Tables **53**, 271 (1993).

[28] Z. H. Levine and S. G. Louie, New model dielectric function and exchange-correlation potential for semiconductors and insulators, Phys. Rev. B **25**, 6310 (1982).

[29] C. D. Archubi, and N. R. Arista, A study of threshold effects in the energy loss of slow protons in semiconductors and insulators using dielectric and nonlinear approaches, Eur. Phys. J. B **89**, 86 (2016).

[30] C. D. Archubi, and N. R. Arista, A comparative study of threshold effects in the energy loss moments of protons, electrons and positrons using dielectric models for band gap materials, Eur. Phys. J. B **90**, 18 (2017).

[31] C. D. Archubi and N. R. Arista, Multiple scattering of slow muons in an electron gas, Eur. Phys. J. D **71**, 239 (2017).

[32] A. D. McLean, and R. S. McLean, Roothaan-Hartree-Fock atomic wave functions Slater basis-set expansions for $Z = 55$-92, At. Data Nucl. Data Tables **26**, 197 (1981).

[33] E. Clementi, and D. Roetti, Roothaan-Hartree-Fock atomic wavefunctions: Basis functions and their coefficients for ground and certain excited states of neutral and ionized atoms, Z=54, At. Data Nucl. Data Tables **14**, 177 (1974).

[34] V. L. Moruzzi, J. F. Janak, and A. R. Williams, *Calculated Electronic Properties of Metals* (Pergamon Press, New York, 1978).

[35] C. C. Montanari, C. D. Archubi, D. M. Mitnik, and J. E. Miraglia, Energy loss of protons in Au, Pb, and Bi using relativistic wave functions, Phys. Rev A **79**, 032903 (2009).

[36] J. E. Valdés, P. Vargas, and N. R. Arista, Electronic energy loss of slow protons channeled in metals, Phys. Rev. A **56**, 4781 (1997).

[37] P. Sigmund, *Particle Penetration and Radiation Effects* (Springer, New York, 2006).

[38] D. G. Arbó, M. S. Gravielle, J. E. Miraglia, J. C. Eckardt, G. H. Lantschner, M Famá, and N. R. Arista, Energy straggling of protons through thin solid films, Phys. Rev. A **65**, 042901 (2002).

[39] Y. Kido, Energy straggling for fast proton beams passing through solid materials, Nucl. Instrum. Methods Phys. Res., Sect. B **24/25**, 347 (1987).

[40] A. Ikeda, K. Sumimoto, T. Nishioka, and Y. Kido, Stopping powers and energy straggling for 50–300 keV H$^+$ in amorphous Si and Ge films, Nucl. Instrum. Methods Phys. Res., Sect. B **115**, 34 (1996).

[41] Y. Kido and T. Koshikawa, Energy straggling for medium-energy H$^+$ beams penetrating Cu, Ag, and Pt, Phys. Rev. A **44**, 1759 (1991).

[42] W. Brandt and R. Laubert, Ionization of the aluminum K shell by low energy hydrogen and helium ions, Phys. Rev. **69**, 178 (1968).

[43] H. Tawara, Y. Achiya, K. Ishii, and S. Morita, K shell ionization of light elements by protons and helium-3-ion impact, Phys. Rev. A **13**, 572 (1975).

[44] J. M. Khan, D. L. Potter, and R. D. Worely, Studies in x-ray production by proton bombardment of C, Mg, Al, Nd, Sm, Gd, Tb, Dy, and Ho, Phys. Rev. **139**, A1735 (1965).

[45] G. Basbas, W. Brandt, and R. Laubert, Universal cross sections for K-shell ionization by heavy charged particles. I. Low particle velocities, Phys. Rev. A **7**, 983 (1973).

[46] G. Basbas, W. Brandt, and R. Laubert, Universal cross sections for K-shell ionization by heavy charged particles. I. Intermediate particle velocities, Phys. Rev. A **17**, 1655 (1978).

[47] W. M. Ariyasinghe, H. T. Awuku, and D. Powers, L-shell ionization of Si, P, S, Cl and Ar by 0.4- to 2.0-MeV H$^+$ and 0.4- to 1.2-MeV H$_2^+$ bombardment, Phys. Rev. A **42**, 3819 (1990).

[48] K. Sera, K. Ishii, M. Kamiya, A. Kuwako, and S. Morita, K-shell ionization of Al and Cu for 0.5-40-MeV-proton bombardment, Phys. Rev. A **21**, 1412 (1980).

[49] K. Ishii, S. Morita, H. Tawara, H. Kaji, and T. Shiokawa, Me-shell ionization of Au, Bi, and U by protons and helium ions in the MeV region, Phys. Rev. A **11**, 119 (1975).